WRF Simulations of the Urban Circulation in the Salt Lake City Area for CO_2 Modeling

THOMAS NEHRKORN, JOHN HENDERSON, MARK LEIDNER, MARIKATE MOUNTAIN, AND JANUSZ ELUSZKIEWICZ

Atmospheric and Environmental Research, Inc., Lexington, Massachusetts

KATHRYN MCKAIN AND STEVEN WOFSY

Harvard University, Cambridge, Massachusetts

(Manuscript received 6 March 2012, in final form 22 August 2012)

ABSTRACT

A recent National Research Council report highlighted the potential utility of atmospheric observations and models for detecting trends in concentrated emissions from localized regions, such as urban areas. The Salt Lake City (SLC), Utah, area was chosen for a pilot study to determine the feasibility of using ground-based sensors to identify trends in anthropogenic urban emissions over a range of time scales (from days to years). The Weather Research and Forecasting model (WRF) was combined with a Lagrangian particle dispersion model and an emission inventory to model carbon dioxide (CO_2) concentrations that can be compared with in situ measurements. An accurate representation of atmospheric transport requires a faithful modeling of the meteorological conditions. This study examines in detail the ability of different configurations of WRF to reproduce the observed local and mesoscale circulations, and the diurnal evolution of the planetary boundary layer (PBL) in the SLC area. Observations from the Vertical Transport and Mixing field experiment in 2000 were used to examine the sensitivity of WRF results to changes in the PBL parameterization and to the inclusion of an urban canopy model (UCM). Results show that for urban locations there is a clear benefit from parameterizing the urban canopy for simulation of the PBL and near-surface conditions, particularly for temperature evolution at night. Simulation of near-surface CO_2 concentrations for a 2-week period in October 2006 showed that running WRF at high resolution (1.33 km) and with a UCM also improves the simulation of observed increases in CO_2 during the early evening.

1. Introduction

Monitoring of current and modeling of future emissions of anthropogenic carbon dioxide (CO_2) are important components of climate change research and policy. Accurate estimates of CO_2 emissions require a combination of approaches: using inventories of known anthropogenic and natural sources (''bottom up'' approach), analyzing flux measurements at selected sites, and combining concentration measurements with transport and dispersion computations to constrain prior estimates of sources (''top down'' approach).

A recent National Research Council (2010) report highlighted the potential utility of atmospheric observations and models for detecting trends in concentrated emissions from localized regions, such as urban areas, where enhancements in greenhouse gas concentrations are readily detectable in the atmosphere. The Salt Lake City (SLC), Utah, area was chosen for a pilot study to determine the feasibility of using ground-based sensors to identify trends in anthropogenic urban emissions over a range of time scales (from days to years). The Weather Research and Forecasting (WRF; Skamarock and Klemp 2008) model was combined with the Stochastic Time-Inverted Lagrangian Transport particle dispersion model (WRF-STILT; Lin et al. 2003; Nehrkorn et al. 2010) and an anthropogenic emission inventory (the Vulcan Project; Gurney et al. 2009) to model CO_2 concentrations, which were then compared with in situ measurements. Computations using this modeling system were performed for four approximately month-long time periods in 2006. Results from that study and their implications for emissions monitoring are described in McKain et al. (2012).

Corresponding author address: Thomas Nehrkorn, AER, 131 Hartwell Ave., Lexington, MA 02421.
E-mail: tnehrkor@aer.com

DOI: 10.1175/JAMC-D-12-061.1

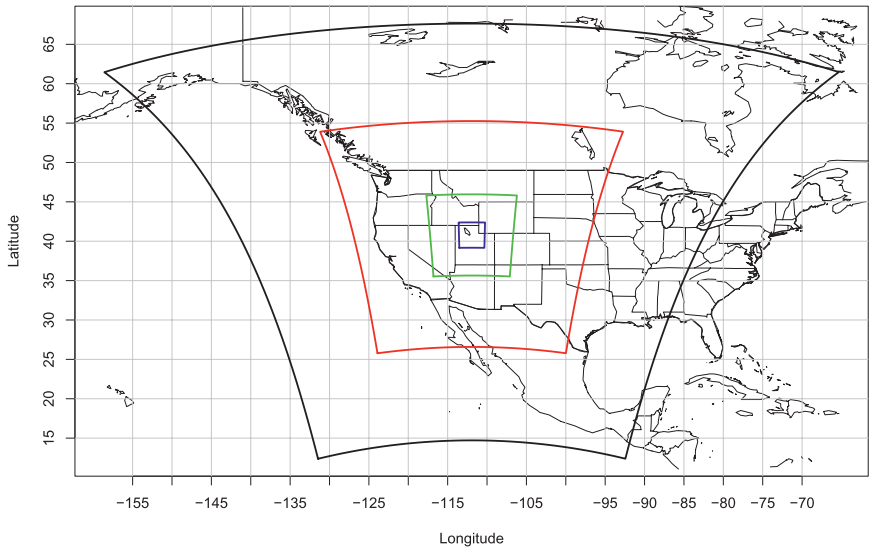

FIG. 1. Outline of the four nested WRF model domains.

In this paper we focus on the role of the WRF mesoscale model in the performance of this urban CO_2 modeling system. In particular, we examine the ability of WRF simulations with varying resolutions and sophistication to reproduce the observed local and mesoscale circulations and the diurnal evolution of the atmospheric boundary layer in the SLC area. Verification of the WRF simulations is performed using both standard meteorological observations from the period covered by our CO_2 simulation and field observations from a field experiment in October of 2000.

The Vertical Transport and Mixing (VTMX; Doran et al. 2002) field-experiment dataset from 2000 provided the opportunity for a detailed assessment of the WRF performance in the SLC area and guided the selection of model configurations for urban CO_2 modeling. A series of sensitivity experiments was performed for two of the VTMX intensive observing periods (IOPs). The WRF configurations were chosen to compare the performance of different PBL schemes with, and without, use of an urban canopy model (UCM; see section 2). On the basis of the results of these comparisons, one configuration was chosen for an evaluation of the end-to-end WRF-STILT modeling system for a selected time period in 2006.

The sensitivity tests complement earlier modeling studies using VTMX data. For example, an intercomparison of different mesoscale-model simulations (Zhong and Fast 2003) found that the three models examined [the fifth-generation Pennsylvania State University–National Center for Atmospheric Research Mesoscale Model (MM5), the Meso Eta Model, and the Regional

TABLE 1. Overview of the WRF configuration that is common to all high-resolution WRF runs. Here, RRTMG is the Rapid Radiative Transfer Model for GCMs; u and v are the east–west and north–south wind components, T is temperature, and q is humidity.

Option	Description
Land surface	Noah (Chen and Dudhia 2001)
Longwave radiation	RRTMG (Iacono et al. 2008)
Shortwave radiation	RRTMG (Iacono et al. 2008)
Microphysics	Lin et al. (Chen and Sun 2002)
Convection	Grell–Devenyi (Grell and Dévényi 2002) (only domains d01 and d02)
Nesting	Two-way, d01 (36 km), d02 (12 km), d03 (4 km), and d04 (1.33 km)
Data assimilation	Use analysis nudging in the outer grid only; perform 30-h forecasts initialized every 24 h (at 0000 UTC), combine hours 7–30 from successive runs for a continuous time series
Nudging	Analysis; u, v, T, and q at all levels above PBL, every 3 h, 1-h relaxation time
Time stepping	Third-order Runge–Kutta; four short time steps per long time step
Advection	Fifth-order horizontal, third-order vertical positive-definite advection for moisture and scalars
Diffusion	Second-order horizontal diffusion using Smagorinsky first-order closure
Damping	No upper-level or vertical velocity damping; default values for divergence and external model damping

TABLE 2. WRF configuration of the high-resolution sensitivity runs. See text for details.

Run name	PBL	Surface layer	Version	Urban land use	UCM
Eddy	YSU	Monin–Obukhov	3.2	1	No
Eddy-L	YSU	Monin–Obukhov	3.2.1	3	No
Eddy-U	YSU	Monin–Obukhov	3.2.1	3	Yes
Turb	MYJ	Monin–Obukhov (Janjić)	3.2	1	No
Turb-U	MYJ	Monin–Obukhov (Janjić)	3.2.1	3	Yes

TABLE 3. Urban land-use categories in NLCD 2001 and their WRF equivalents. Also shown is the urban fraction assigned to each WRF urban category.

NLCD		WRF		
No.	Description	No.	Description	Urban fraction
21	Developed, open space	31	Low-density residential	0.50
22	Developed, low intensity	31	Low-density residential	0.50
23	Developed, medium intensity	32	High-density residential	0.90
24	Developed, high intensity	33	Industrial or commercial	0.95

Atmospheric Modeling System (RAMS)] were each successful at reproducing the general aspects of the mesoscale circulation, but all had important deficiencies in capturing the diurnal cycle of the near-surface temperature. That study examined the same IOPs (7 and 10) used in the study presented here. The performance of a high-resolution version of the Coupled Ocean–Atmosphere Mesoscale Prediction System (COAMPS) model with a multilayer UCM was examined by Chin et al. (2005) for IOP 10. They found that including the UCM improved some aspects of the simulations (in particular, winds), but not others (temperature).

The modeling tools, input and verification datasets, and experimental design are described in the next section. Results from the WRF sensitivity tests with VTMX field-experiment verification data are described in section 3a. Results from WRF simulations for 2006, using both a low-resolution configuration and one of the tested high-resolution configurations with a UCM, are described in section 3b. The implications of these results for modeling and monitoring of urban emissions of CO_2 are discussed in section 4.

2. Models, data, and experimental design

a. WRF configuration

The Advanced Research version of the WRF model was used for these experiments. A total of four nested domains, with resolutions down to 1.33 km, were centered over the SLC area (Fig. 1). WRF was run with only the three outer domains for most simulations during 2006; this configuration is referred to as low resolution in the following. For the VTMX sensitivity runs, all four domains were used. All WRF runs used 41 vertical levels, with 11 layers below 2 km. The North American Regional Analysis (NARR) was used to provide initial and lateral boundary conditions for all WRF runs. A summary of WRF configurations common to all high-resolution WRF runs is shown in Table 1. For the WRF sensitivity runs, the effect of varying the planetary boundary layer (PBL) parameterization and the urban surface were investigated by conducting the sensitivity test runs summarized in Table 2. Two PBL schemes were selected as the most widely used representatives of first-order and higher-order turbulence closure schemes: the Yonsei University model (YSU; Hong et al. 2006), a first-order-closure, eddy-diffusivity turbulence scheme that incorporates the effects of nonlocal mixing (hereinafter Eddy), and the Mellor–Yamada–Janjić technique (MYJ; Mellor and Yamada 1982; Janjić 2002), a 1.5-order-closure scheme that is based on prognostic turbulent kinetic energy (hereinafter Turb). The low-resolution WRF runs used the same configuration as shown in Table 1 (except only for domains d01–d03) and the eddy configuration shown in Table 2 (except that version 3.1.1 of WRF was used for low-resolution runs). Comparisons in the literature among YSU, MYJ, and other PBL schemes have been conducted for different locations and times of year, with varying results. For example, Otkin and Greenwald (2008) found insufficient vertical mixing, particularly for the MYJ scheme, in simulations over the North Atlantic Ocean, whereas Bowman (2009) noted too much mixing in simulations of the mountainous Pacific Northwest, regardless of the PBL scheme, in both MM5 and WRF. In summertime simulations over the central United States, Hu et al. (2010) attributed larger positive temperature and negative moisture biases in MYJ (as compared with YSU) to an underestimate of vertical mixing caused by the lack of nonlocal mixing in the MYJ scheme.

For an accurate representation of the urban environment, it is necessary to incorporate interactions between the urban landscape (e.g., residential and commercial buildings of varying heights and paved surfaces) and the overlying atmosphere. While a detailed treatment of flow around individual buildings cannot be represented in a mesoscale model, bulk effects of the urban ''canopy'' (in analogy to vegetative canopies such as forests)

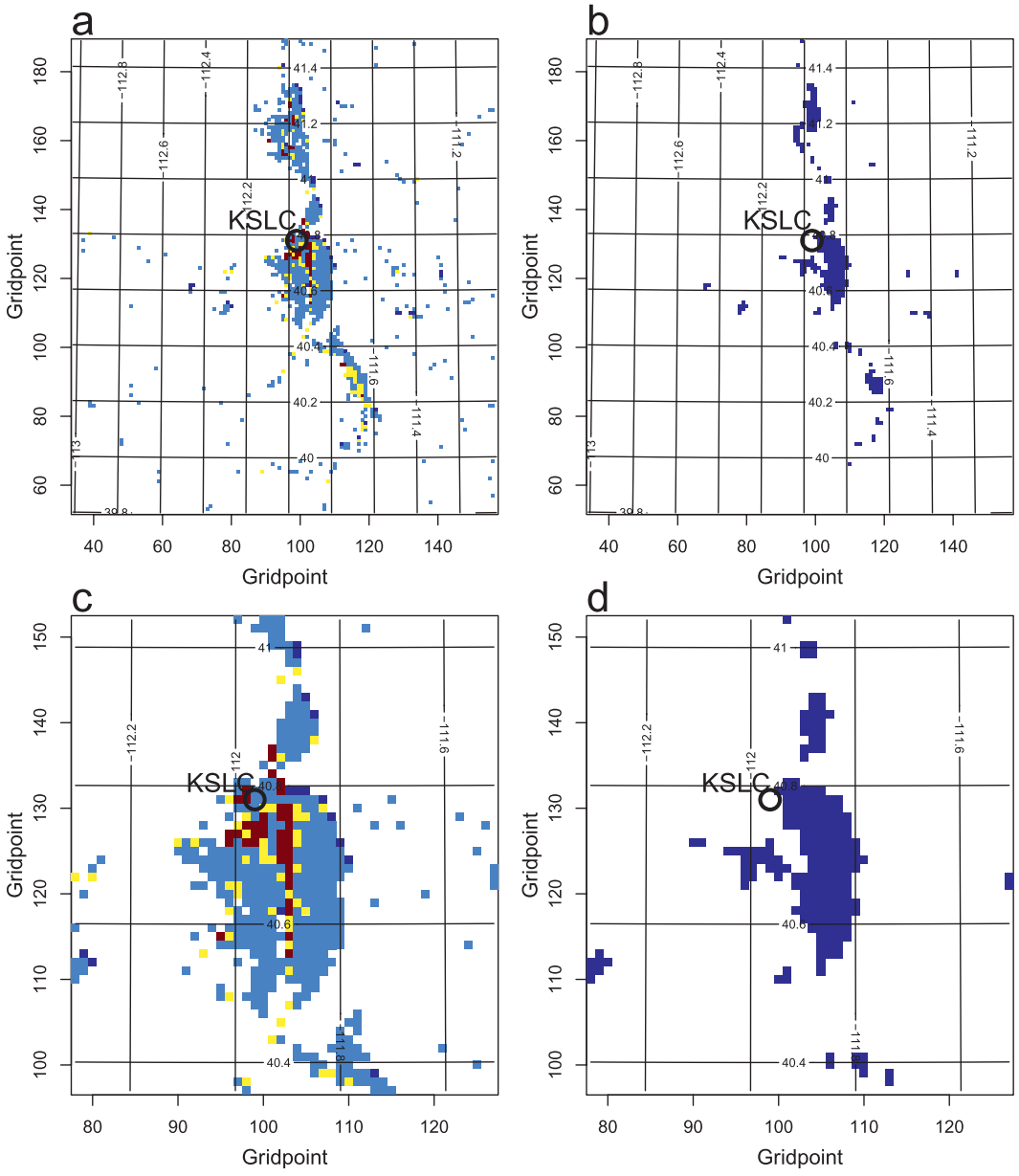

FIG. 2. Urban land-use categories in (a),(c) LU33 and (b),(d) LU24 for (top) the central part of d04 encompassing the Provo, Salt Lake City, and Ogden (Utah) urban areas and (bottom) a close-up for SLC. Axis labels are gridpoint indices in d04, latitude and longitude are shown as grid lines, and the location of the Salt Lake City airport is the circle marked KSLC. Grid boxes are colored to indicate land use: dark blue (single urban category used in LU24), light blue (low-density residential), yellow (high-density residential), and red (commercial/industrial).

can be represented by UCMs. WRF includes two options for UCMs: one is a single-layer treatment, which was chosen for this study. The other is a multilayer parameterization, which would require very high vertical resolution within the PBL and which is only compatible with the Boulac (Bougeault and Lacarrere 1989) second-order PBL scheme. An intercomparison of the WRF single- and multilayer UCMs within the COAMPS model for the New York City, New York, area (Holt and Pullen 2007) found no advantage of the added complexity and computational expense associated with the multilayer scheme. In a more recent study for the Houston, Texas, area Salamanca et al. (2011) found that single-layer schemes in WRF are sufficient unless anthropogenic heat sources due to air conditioning are a significant factor (which is not applicable to Salt Lake City in October). A detailed description of the single-layer UCM is provided in Chen et al. (2011).

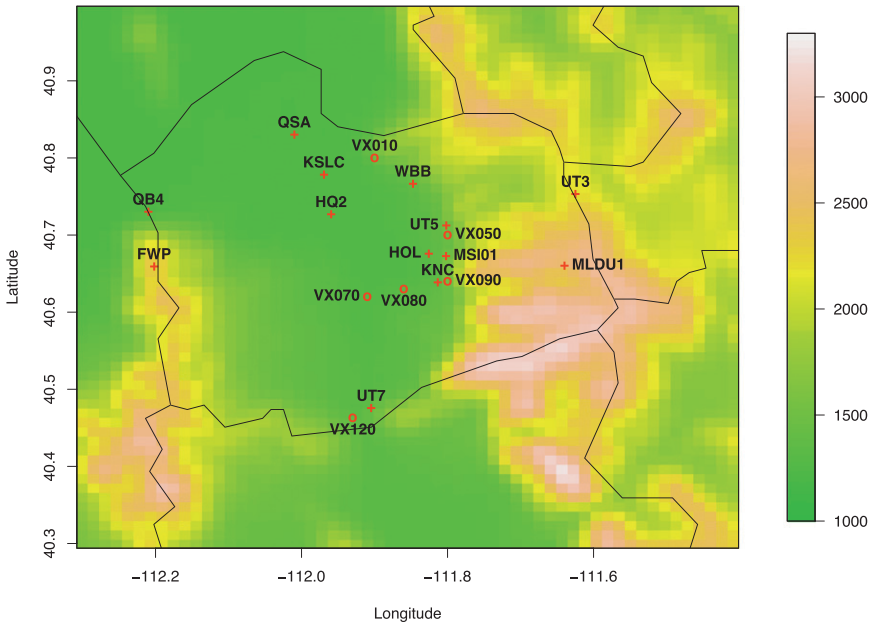

FIG. 3. WRF terrain height map (m MSL) of the Salt Lake valley with VTMX upper-air stations noted as circles and Mesowest surface stations noted as plus signs. County boundaries are shown as black lines.

Our experimental design includes two runs for each choice of the PBL scheme: one with the single-layer urban canopy parameterization (UCM) and one without it. (Hereinafter, the suffix -U is added to the corresponding UCM experiment name.) The two high-resolution runs without the UCM were completed with WRF, version 3.2. Runs with the UCM were completed with version 3.2.1, because the newer version included improvements specifically for the UCM. To take advantage of the UCM's capabilities, it is important to correctly specify a large number of parameters that characterize the interaction between the urban landscape and the overlying atmosphere. Loridan et al. (2010) examined the response of the WRF UCM to changes in these parameters in an in-depth sensitivity study. For the current study, initialization of these parameters was based on the default parameters established for three categories of urban land-use types (Chen et al. 2011). Loridan and Grimmond (2012) more recently examined the performance of the WRF single-layer UCM in conjunction with the "Noah" surface layer parameterization (Chen and Dudhia 2001) in offline tests, using a variety of methods to specify the UCM parameters. A key parameter is the urban fraction of each grid cell (see Table 3), which determines the partitioning of surface fluxes between the urban (as computed by the UCM) and vegetated (as computed by Noah) portions. Loridan and Grimmond (2012) suggested the use of three urban categories, assigned to grid cells on the basis of morphological criteria (e.g., fraction of vegetated area) or observed flux ratios, and a new set of associated default UCM parameters. In the next section we describe the high-resolution land-use dataset needed for that application.

b. *Land-use datasets*

A high-resolution (1″, or approximately 30 m) land-use dataset that is based on 2001 National Land Cover Data (NLCD 2001) was obtained from the Multi-resolution Land Characteristics Consortium (MRLC; www.mrlc.gov). The MRLC dataset is based primarily on *Landsat-5* and *-7* imagery and is described in detail in Homer et al. (2004). It includes four urban land-use categories, which are determined by first applying an urban mask derived from ancillary datasets (population density, U.S. Census Bureau road data, and satellite-derived nighttime light data), followed by an urban density classification that is based on imperviousness derived from Landsat spectral data [for additional details, see Yang et al. (2003)]. These four NLCD land-use categories were assigned to one of three urban categories in WRF with corresponding urban fractions (Table 3). For the UCM simulations only, the land-use index values of grid points (within the area covered by domain d04) were modified to one of the three urban categories where applicable. The resulting blended land-use dataset is denoted by LU33, and the original land-use dataset (which contains just a single urban land-use category) is denoted by LU24. Comparison of the urban

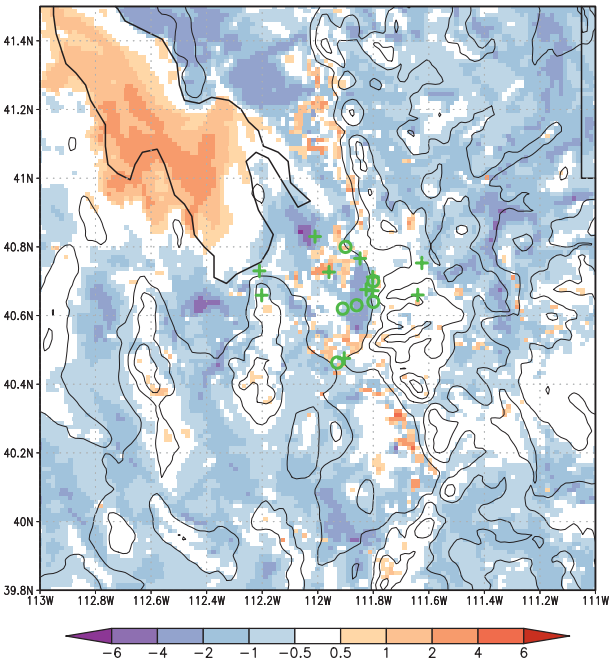

FIG. 4. The 2-m temperature differences (°C) between the Eddy configurations Eddy-U (UCM) minus Eddy (no UCM; old land use), just before sunrise on 18 Oct (1200 UTC). Terrain height is contoured in light gray every 500 m. As in Fig. 3, VTMX upper-air stations are plotted as circles and Mesowest surface stations are plotted as plus signs.

regions of LU24 and LU33 (Fig. 2) shows that the new LU33 dataset adds considerable detail to the definition and extent of the urban regions in domain d04. In particular, low-density residential areas were added to previously nonurban grid points on the western side of SLC, most previous single-category urban grid points were replaced with low-density residential grid points, and high-density residential and commercial/industrial areas were added in the downtown area. The differences in the land-use maps are important in the innermost domain d04, but they are less significant in domains d01–d03 (not shown). In d01, the land-use differences appear as only several pixels within the entire domain. To isolate the effects of the updated WRF version and land-use dataset from those of the UCM, an additional experiment (Eddy-L) was conducted that was identical to Eddy-U in all respects except that the UCM was not activated.

c. *VTMX data*

The VTMX was a multi-institutional campaign that was conducted in the vicinity of Salt Lake City during October of 2000 (Doran et al. 2002) and provided the means for verifying upper-air fields of the different high-resolution WRF configurations listed in Table 2. A goal of the VTMX program (Doran et al. 2002) was to better understand the meteorological processes affecting transport and mixing in the atmosphere, with a focus on the nocturnal stable periods and the morning and evening transition periods, especially in urban valley areas. Doran et al. (2002) grouped the IOPs into two categories on the basis of the amount of modulation by the synoptic-scale flow on the smaller-scale drainage circulations, and one IOP from each category was selected for this study. IOP 7, from 2200 UTC 17 October to 1600 UTC 18 October, was characterized by quiescent synoptic-scale flow until about 1200 UTC yet sufficient insolation thereafter such that robust valley and mountain breezes developed (Zhong and Fast 2003). In contrast, daytime cloud cover and southerly surface winds associated with the approach of a synoptic-scale trough during IOP 10 (2200 UTC 25 October–1600 UTC 26 October) substantially reduced local effects.

Figure 3 shows the locations of VTMX upper-air stations and those Mesowest surface stations that underwent strong quality control. The three rawinsondes and three radar wind profilers available for IOPs 7 and 10 were located at different sites throughout the Salt Lake Valley. The rawinsondes (VX010, VX080, and VX120), located at the north end, center, and south end of the valley, respectively, provided profiles of wind, temperature, and humidity. Rawinsonde data frequency ranged from 1 to 4 h.

3. Results

WRF forecasts for the VTMX cases during October of 2000 are evaluated using the available field-experiment datasets to determine which model setup provides the best overall simulation of meteorological conditions, particularly for driving models of atmospheric transport and dispersion (section 3a). Evaluations using standard meteorological observations during a 2-week period in October of 2006 (section 3b) provide an indication as to what extent these results are representative for the time period of interest for CO_2 simulations.

a. *October 2000 sensitivity experiments*

A good indication of the sensitivity of WRF forecasts to the different model configurations is provided by an examination of spatial differences in near-surface variables that are important to atmospheric dispersion. Differences have been examined in 2-m temperature, PBL height, and 10-m wind speed.

The most pronounced and repeatable differences between model configurations are seen in the 2-m temperatures during the overnight hours. Figure 4 shows the differences in 2-m temperature between UCM and non-UCM forecasts for the Eddy configuration in the early

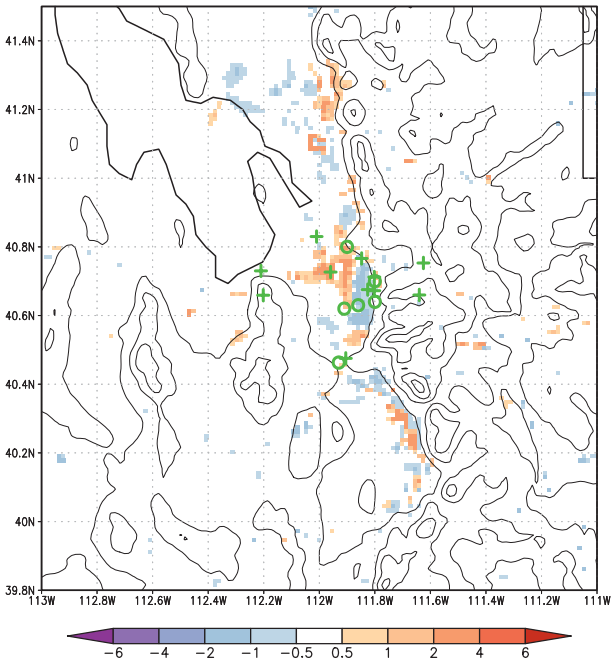

FIG. 5. As in Fig. 4, but between the Eddy configurations, Eddy-U (UCM) minus Eddy-L (no UCM, but same land use and WRF version as Eddy-U).

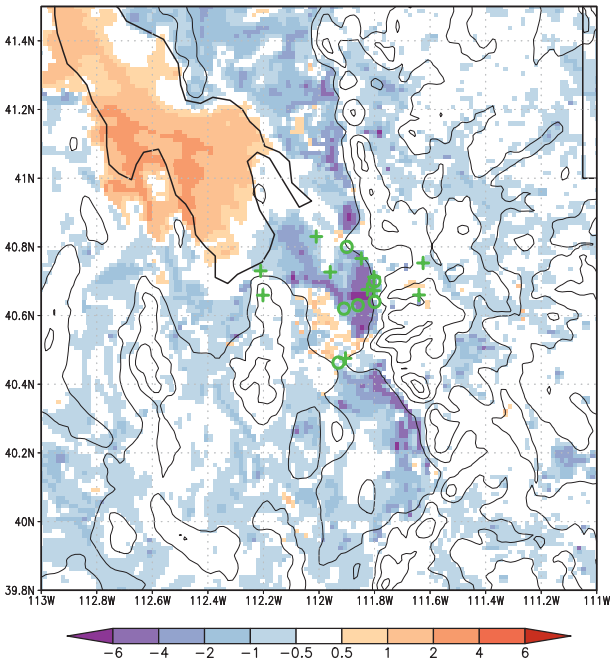

FIG. 6. As in Fig. 4, but for differences between the Turb configurations, UCM minus no UCM.

morning hours of 18 October (IOP 7). The consistent positive temperature differences over the Great Salt Lake and the mostly negative differences over nonurban land areas are related to changes in model versions (3.2 vs 3.2.1) rather than the UCM, since these differences are absent in Fig. 5, which shows the differences between the Eddy-U and Eddy-L configurations. Around the SLC area, the early-morning temperatures are predominantly colder using the UCM, because large urban areas were converted to low-density residential (light blue in Fig. 2) from their prior, single urban classification (dark blue in Fig. 2). A comparison with Fig. 5 shows that both the cooler temperatures in the eastern part of SLC and the warmer temperatures in the central part of SLC have a substantial component that is due to the use of the UCM. Although many potential factors play a role in how the UCM will respond to different urban surface types (e.g., Loridan and Grimmond 2012), a key influence is likely that low-density residential areas will cool faster at night than in the prior, single urban classification because the surface emissivity is higher. There are scattered positive differences in the Salt Lake City urban area (orange and red grid points in Fig. 4). These

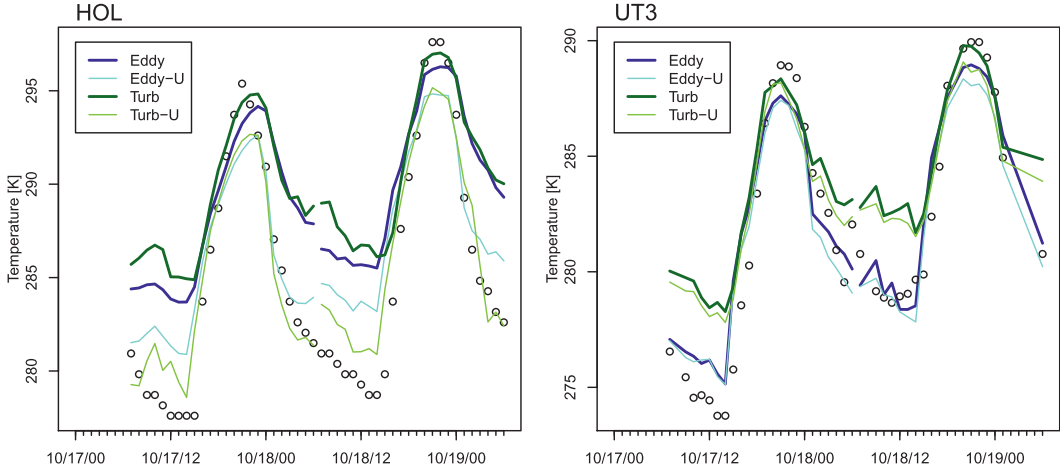

FIG. 7. Time series of forecast and observed temperatures for the (left) HOL and (right) UT3 stations for IOP 7.

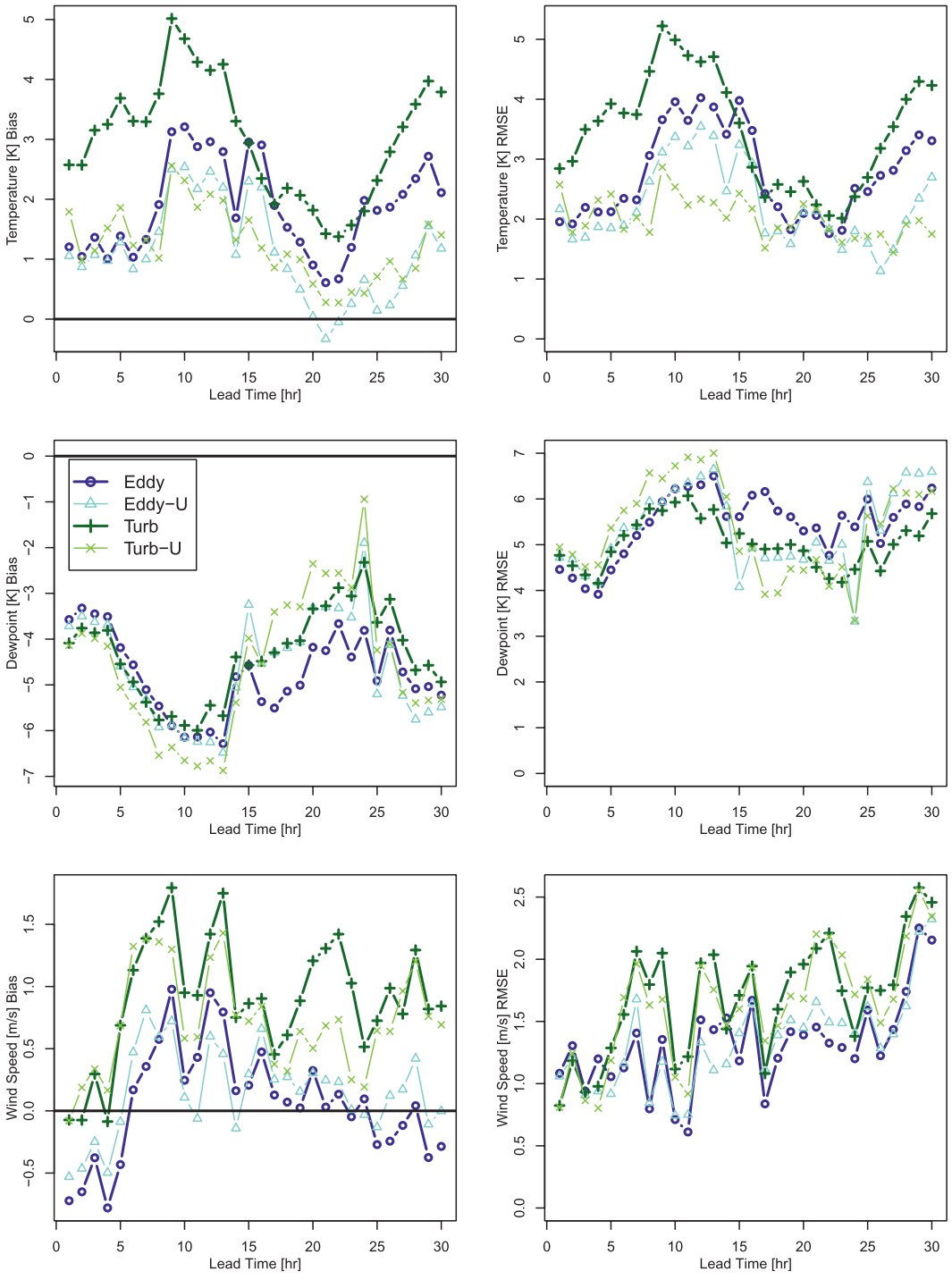

FIG. 8. IOP-7 (left) surface bias and (right) RMSE for (top) temperature, (middle) dewpoint, and (bottom) wind speed for each of the four treatments: Eddy (dark blue), Eddy-U (light blue), Turb (dark green), and Turb-U (light green).

correspond to grid points that were reclassified as low-density residential from some nonurban category or that were reclassified as high-density residential or industrial/commercial in the LU33 classification (yellow and red in Fig. 2). The 2-m temperature differences for the Turb-U versus Turb runs are shown in Fig. 6. The UCM leads to a more pronounced cooling over eastern SLC and less warming over the central SLC area in this case.

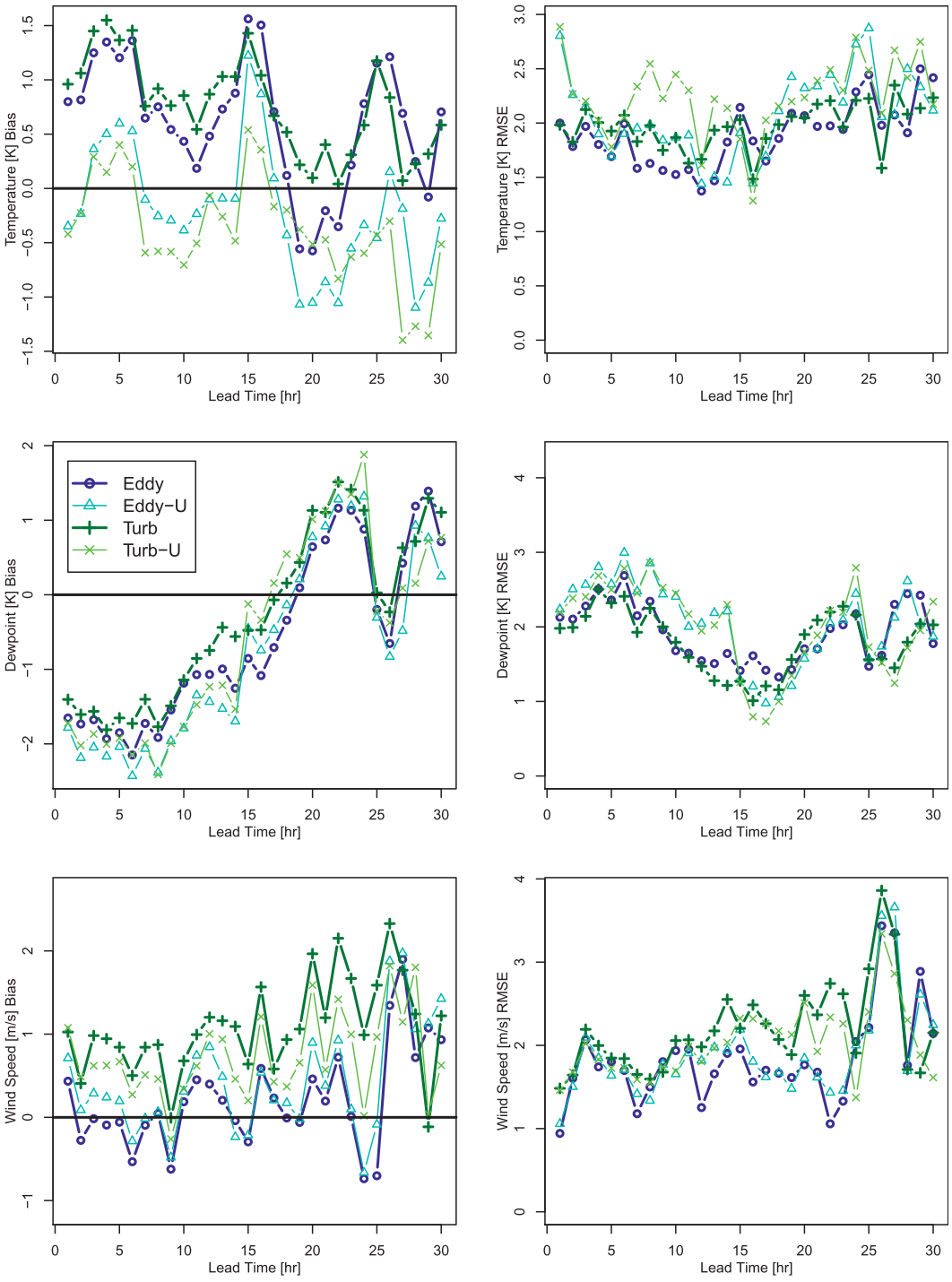

FIG. 9. As in Fig. 8, but for IOP 10.

An intercomparison of all four runs is depicted in Fig. 7, which shows the diurnal cycle of 2-m temperature during IOP 7 at Mesowest stations in an urban area (HOL) and in a rural area (UT3). At the urban location, the nighttime temperatures in the Turb (shown in green) runs are warmer relative to the Eddy PBL scheme (shown in blue)—a difference that is seen in general in the urban areas. The more pronounced UCM-induced cooling (light vs dark lines) more than compensates for this difference, resulting in Turb-U nighttime

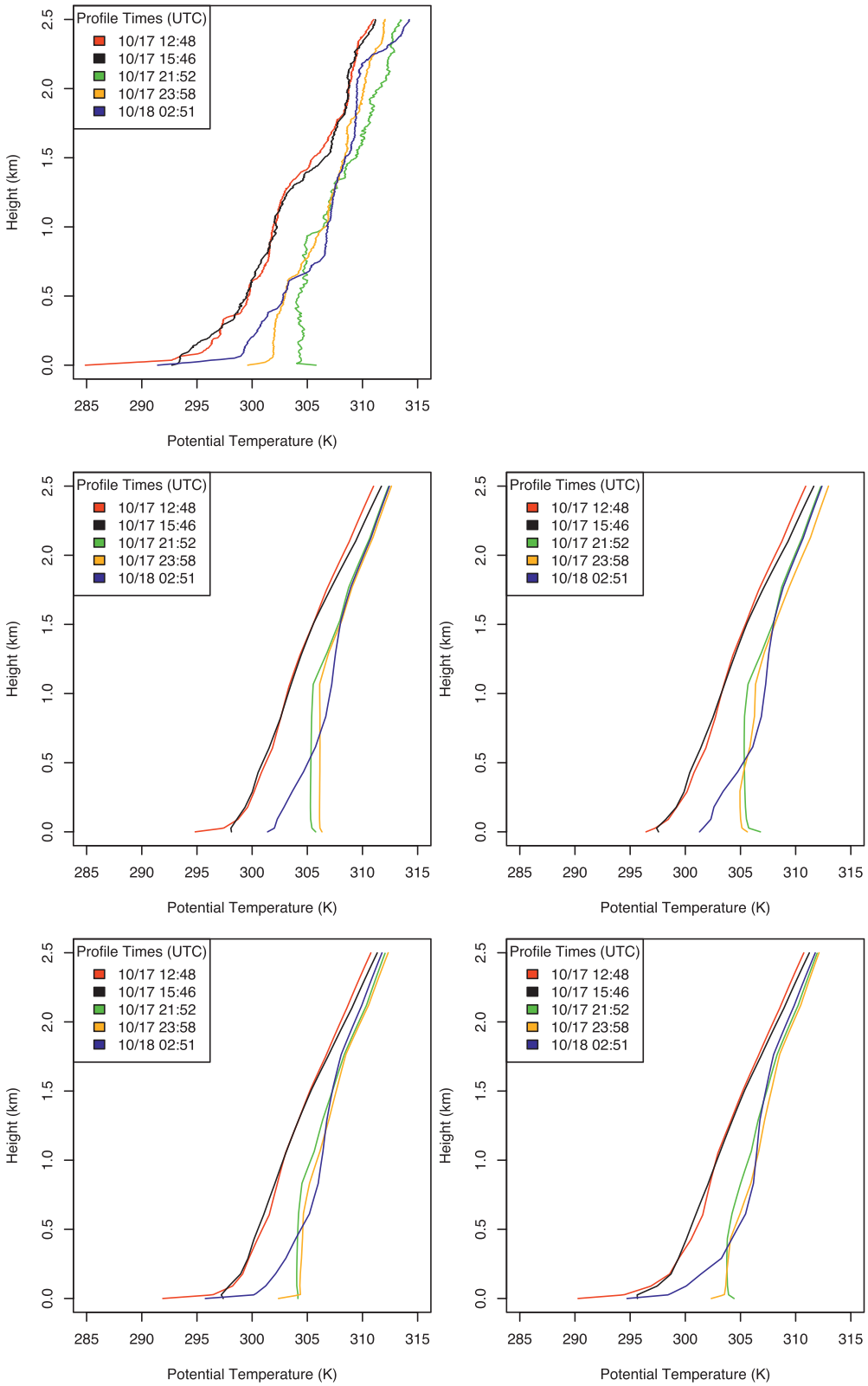

FIG. 10. VX080 IOP-7 potential temperature profile plot at different sounding times for (top left) observations, (middle left) Eddy, (bottom left) Eddy-U, (middle right) Turb, and (bottom right) Turb-U.

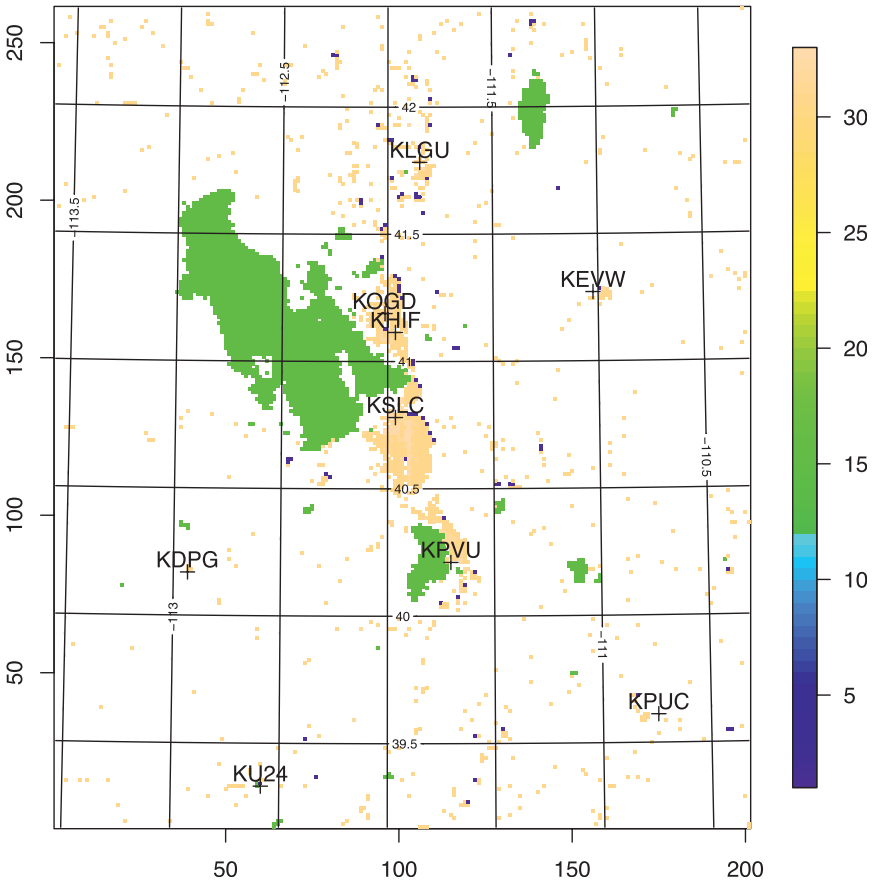

FIG. 11. Location of NWS surface stations in the innermost domain used for verification for October 2006. Axes are labeled with gridpoint indices, latitude and longitudes are shown as grid lines, and pixels are colored by land-use index according to the color scale, but for clarity only grid points over water (16) and in urban settings (1 and 31–33) are colored.

temperatures that are the coldest of all four configurations and that are the closest to the observations in this case. As is to be expected, the UCM makes little difference at the rural location, and here both Eddy runs produce the coolest nighttime temperatures, in better agreement with the observations than are the Turb runs.

In contrast to the differences in overnight temperatures, daytime temperature differences between UCM and non-UCM model configurations, forced by solar heating and homogenized by boundary layer mixing, are much smaller (less than 1°–2°C; not shown), regardless of PBL scheme. This is also evident in the time series at individual locations (Fig. 7).

The changes in 2-m temperatures are also reflected in corresponding differences in boundary layer height. Because the PBL typically collapses at night without solar heating of the surface, differences in PBL height between the model configurations are minimal at night. During the day, when the PBL depth is maintained by solar forcing, nonstationary, transient differences of up to a few hundred meters, both positive and negative, are present across the 1.33-km grid (not shown). As is the case for daytime temperatures, no significant systematic differences are apparent.

Spatial statistics were computed over all Mesowest stations with data that underwent strong quality-control measures (5–10 stations). Figures 8 and 9 depict bias and root-mean-square errors (RMSE) for 2-m temperature, 2-m dewpoint temperature, and 10-m wind speed for IOPs 7 and 10, respectively. For IOP 7, the UCM runs (light colors) have a smaller positive bias relative to the non-UCM runs (dark colors), particularly during the evening and nighttime periods: 8–15 and 24–30 h, respectively. This nocturnal difference is also reflected in the RMSE. This statistical result confirms the spatial difference pattern shown in Figs. 4 and 6 and the individual station results shown in Fig. 7. In contrast, for the synoptically disturbed IOP 10 (Fig. 9) the non-UCM temperature bias is smaller and the cooler UCM-run temperatures result in negative biases of similar

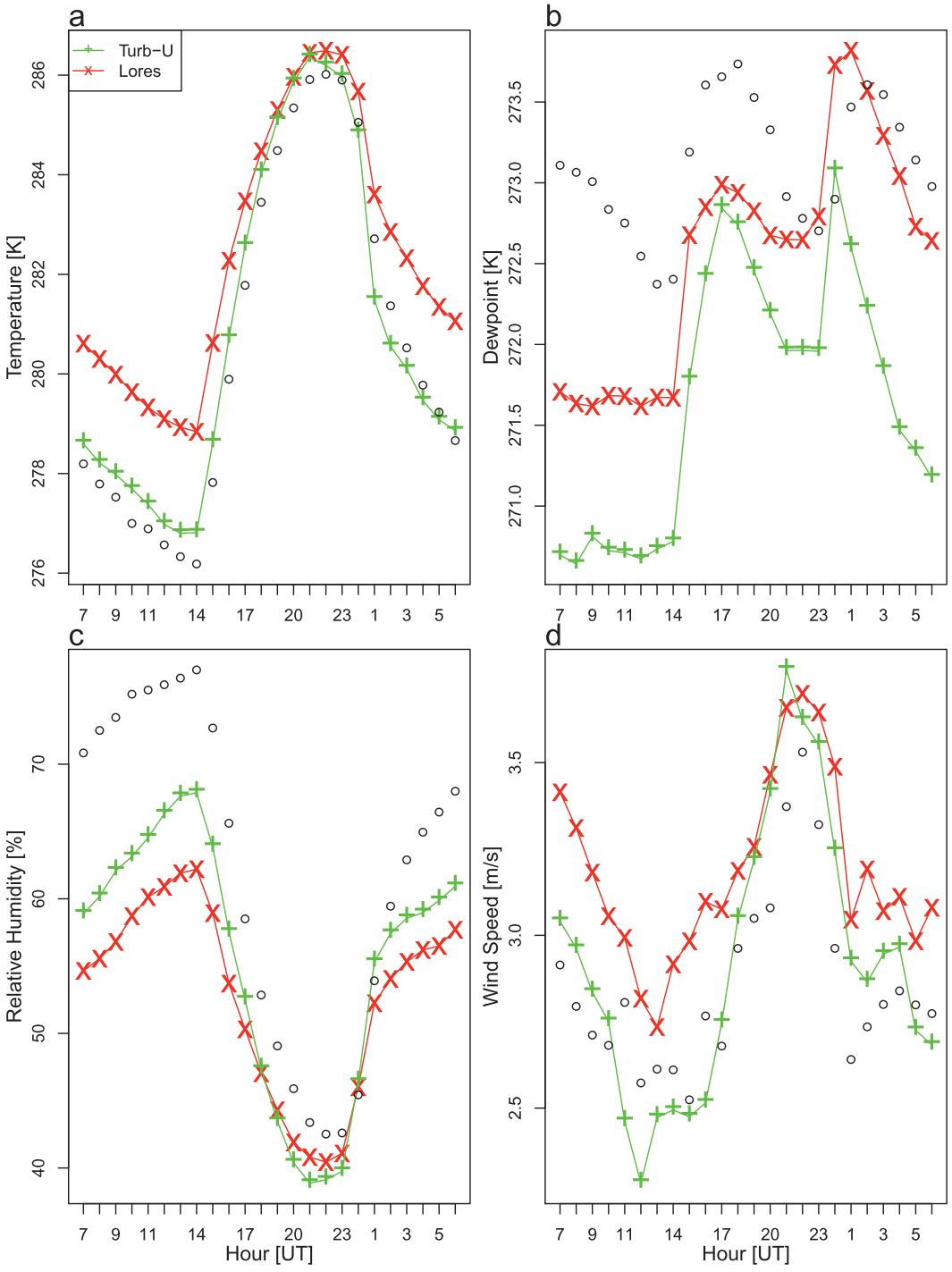

FIG. 12. Observed and low-resolution and Turb-U mean simulated values of (a) temperature, (b) dewpoint, (c) relative humidity, and (d) wind speed, as a function of time of day (UTC), averaged over all NWS surface stations and all available days during October 2006.

magnitude. As a result, the RMSE is virtually identical for all experiments for IOP 10.

The RMSE and bias for wind fields are similar for runs using the same PBL scheme (unlike what was seen for temperature): dark and light lines of the same color tend to group together in the wind speed panels in Figs. 8 and 9. Overall, differences between the experiments are smaller for these fields than for temperature, with only

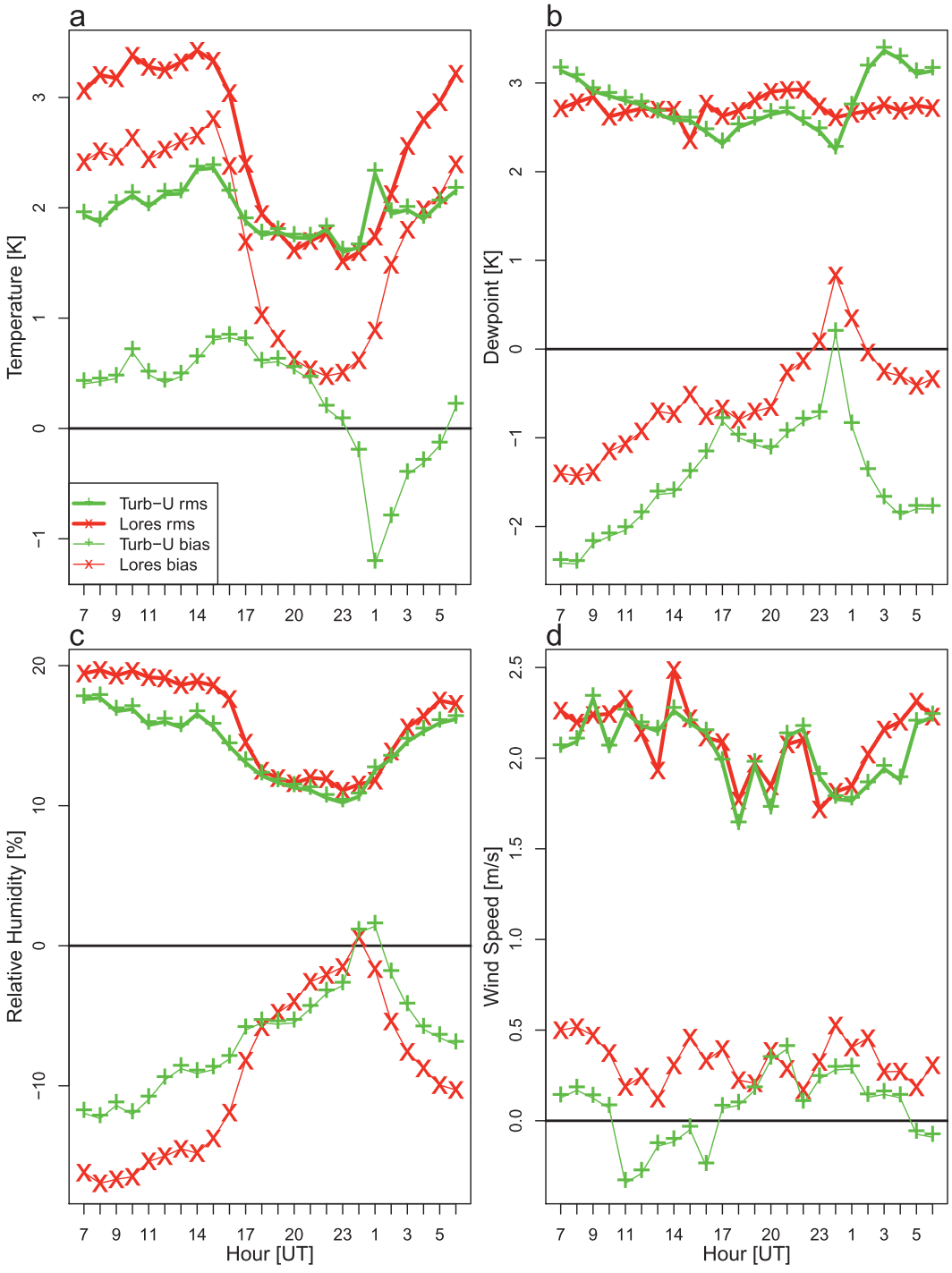

FIG. 13. Low-resolution and Turb-U RMSE (heavy lines) and bias (light lines) of (a) temperature, (b) dewpoint, (c) relative humidity, and (d) wind speed, as a function of time of day (UTC), averaged over all NWS surface stations and all available days during October 2006.

a slightly smaller bias and RMSE for the runs with the Eddy PBL scheme (YSU). All WRF simulations captured the terrain-induced local circulations (slope and valley winds) that were especially pronounced during the synoptically quiescent IOP 7 (not shown here). The wind speed biases shown in Figs. 8 and 9 are relatively small overall (most are less than 1 m s^{-1}). Jiménez and Dudhia (2012) found higher biases in WRF simulations

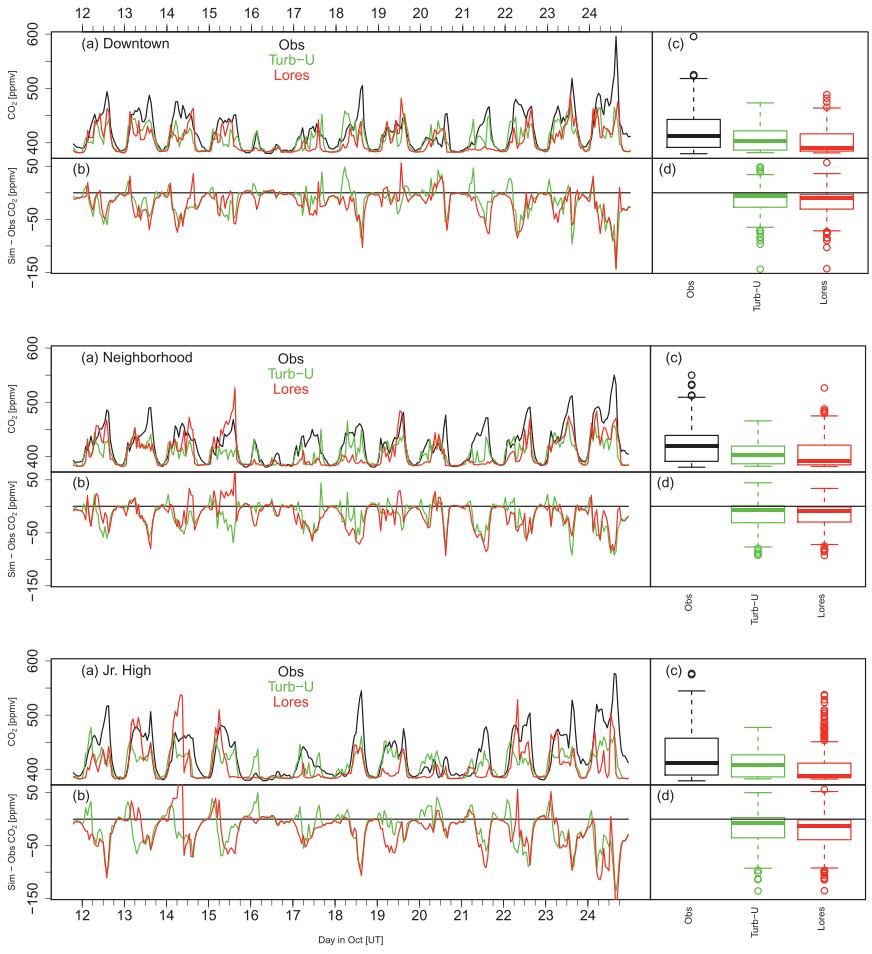

FIG. 14. Time series of hourly mean observed and modeled CO_2 concentrations for 2 weeks in October 2006, for three sites in SLC (top, downtown; middle, neighborhood; bottom, junior high school). For each site, the top-left plot shows the simulated values, the bottom-left plot shows the corresponding errors, and the top- and bottom-right panels show boxplots of values and errors, respectively. The boxes enclose the first and third quartiles, the horizontal line marks the median, the whiskers extend to the range of data points within 1.5 of the interquartile range from the boxes, and outliers beyond the whiskers are plotted as circles.

in complex terrain at higher wind speeds and suggested an improved parameterization for near-surface wind speeds. The small sample size precludes an analysis of wind speed bias as a function of wind speed in our case, and it remains to be determined whether the near-surface wind speeds would be improved by this parameterization in our case.

The error statistics for dewpoint temperature are virtually identical for all experiments. For IOP 7, all experiments exhibit large negative biases, possibly caused by an incorrect partitioning between latent and sensible heat fluxes (since temperature biases are positive), which could be related to underestimates of soil moisture (these are initialized from NARR analysis values). During IOP 10 the moisture bias changes monotonically throughout the period (changing sign by 1900 UTC), reflecting errors in the synoptic trends during that time.

The spatial statistics suggest that the UCM treatments are better at modeling surface temperature during calm events driven by local circulations. In the wind fields, the spatial statistics indicate that treatments with a YSU PBL scheme may have a slight advantage, but the small sample size prevents a clear conclusion of which PBL scheme performs better.

VTMX data from three rawinsonde sites and three radar wind profiler sites were used to verify the upper-air fields (winds and temperature) of the four WRF forecasts for both IOPs. All WRF runs captured the main features of the observed wind fields (not shown),

TABLE 4. Error statistics of simulated CO_2, at the three measurement sites and overall, for the Turb-U and LoRes cases. Here, *N* is the sample size, bias is the mean error, RMSE is the root-mean-square error, corr is the correlation coefficient, and slope is the reduced major-axis regression-line slope; DT, NH, and JH indicate the downtown, neighborhood, and junior high school sites, respectively.

Site	Case	*N*	Bias (ppmv)	RMSE (ppmv)	Corr	Slope
DT	LoRes	317	−17.74	29.66	0.70	0.69
DT	Turb-U	317	−13.35	27.35	0.70	0.65
NH	LoRes	317	−15.75	28.65	0.70	0.83
NH	Turb-U	317	−15.25	27.83	0.71	0.60
JH	LoRes	317	−20.82	39.03	0.61	0.77
JH	Turb-U	317	−16.07	34.12	0.69	0.55
All	LoRes	951	−18.10	32.78	0.66	0.77
All	Turb-U	951	−14.89	29.93	0.70	0.59

and there were no significant differences among the wind fields of the different WRF runs. Potential temperature profiles for VX080 during IOP 7 are shown in Fig. 10. There is a very sharp nocturnal surface inversion early on both 17 and 18 October, as seen in the sharp gradient near the surface. This feature is not fully resolved in any of the WRF runs, but the potential temperature profiles of the UCM runs are closer to the observed profiles, with a sharper curvature, partly due to more accurate near-surface temperatures. In some cases the nocturnal surface temperature is at least 5°C cooler than the non-UCM treatment. The timing of the erosion and reforming of the nocturnal surface inversion is notably improved in the UCM runs: both the observations and the UCM runs show the nocturnal inversion forming around 0000 UTC 18 October, whereas in the non-UCM this is delayed until around 0300 UTC 18 October, a full 3 h later. It is also notable that PBL heights during the heat of the day in non-UCM forecasts are too deep when compared with observations. Without the urban parameterization, the WRF surface temperatures are too warm and result in boundary layers that are too deep. This indicates that the UCM is crucial to accurately model the surface temperature and boundary layer, particularly at night, during IOP 7.

During IOP 10 the nocturnal surface inversion is much weaker, and the difference between the UCM and non-UCM configurations is almost indiscernible (not shown). Here, the choice of PBL scheme exerts a larger influence, with slightly better agreement with observations for the runs with the Turb PBL scheme (MYJ).

b. October 2006 low- and high-resolution runs

The WRF-STILT modeling system was used for four separate seasons during 2006 to simulate the CO_2 measurements taken in the SLC area during this time. The low-resolution configuration of WRF was used for all of these calculations. To determine the improvement possible from a high-resolution version of WRF, computations were also performed using the Turb-U configuration for a 2-week period during October of 2006 (10–24 October). Verification statistics of the WRF-simulated meteorological conditions were computed against the standard National Weather Service (NWS) observation station data in the innermost domain. As is evident from Fig. 11, the majority of these stations are located in or near urban locations. The results showed that the beneficial effects of the high-resolution, UCM WRF configuration are also evident for this time period. The mean diurnal cycle of temperature at those locations is much closer to the observations for the Turb-U run than for the low-resolution WRF run (Fig. 12), particularly during the nighttime hours. Some improvement is also evident in the mean wind speeds, whereas the results are inconclusive for moisture: dewpoints exhibit larger (negative) biases (but they are much smaller than at the VTMX stations during IOP 7), but because of the improved temperature bias, there is an improvement in the mean relative humidity values. Similarly, the root-mean-square errors (Fig. 13) show a noticeable improvement in temperature for Turb-U, with largely neutral impacts for wind speed and dewpoint and a slight positive impact for relative humidity.

The improved meteorological fields produced by the high-resolution (Turb-U) WRF configuration had a noticeable effect on the simulated near-surface CO_2 concentrations. The simulated concentrations are the sum of average background observations and hourly modeled enhancements, which include inputs from anthropogenic and biospheric flux fields [see McKain et al. (2012) for details]. Hourly observed values (shown in black in Fig. 14) are the mean of the raw, 5-min observations. Time series of modeled values resulting from both the baseline (4-km resolution, hereinafter LoRes) meteorological configuration and the high-resolution (1.33 km) configuration with the urban canopy model (Turb-U) are shown in Fig. 14 alongside the observations. The time series demonstrate a small, but consistent, improvement. These improvements are also reflected in the error statistics shown in Table 4.

The mean diurnal cycle (Fig. 15) shows that the improvements at two of the three measurement sites (''downtown'' and ''neighborhood'') primarily stem from an improved representation of the late-afternoon/early-nighttime (1800–2300 mountain standard time; 0100–0600 UTC) rise in concentrations, consistent with the improved modeling of the afternoon PBL collapse seen for October 2000 (Fig. 10), and of the improved near-surface temperatures (Fig. 8) at that time of day. Both sets

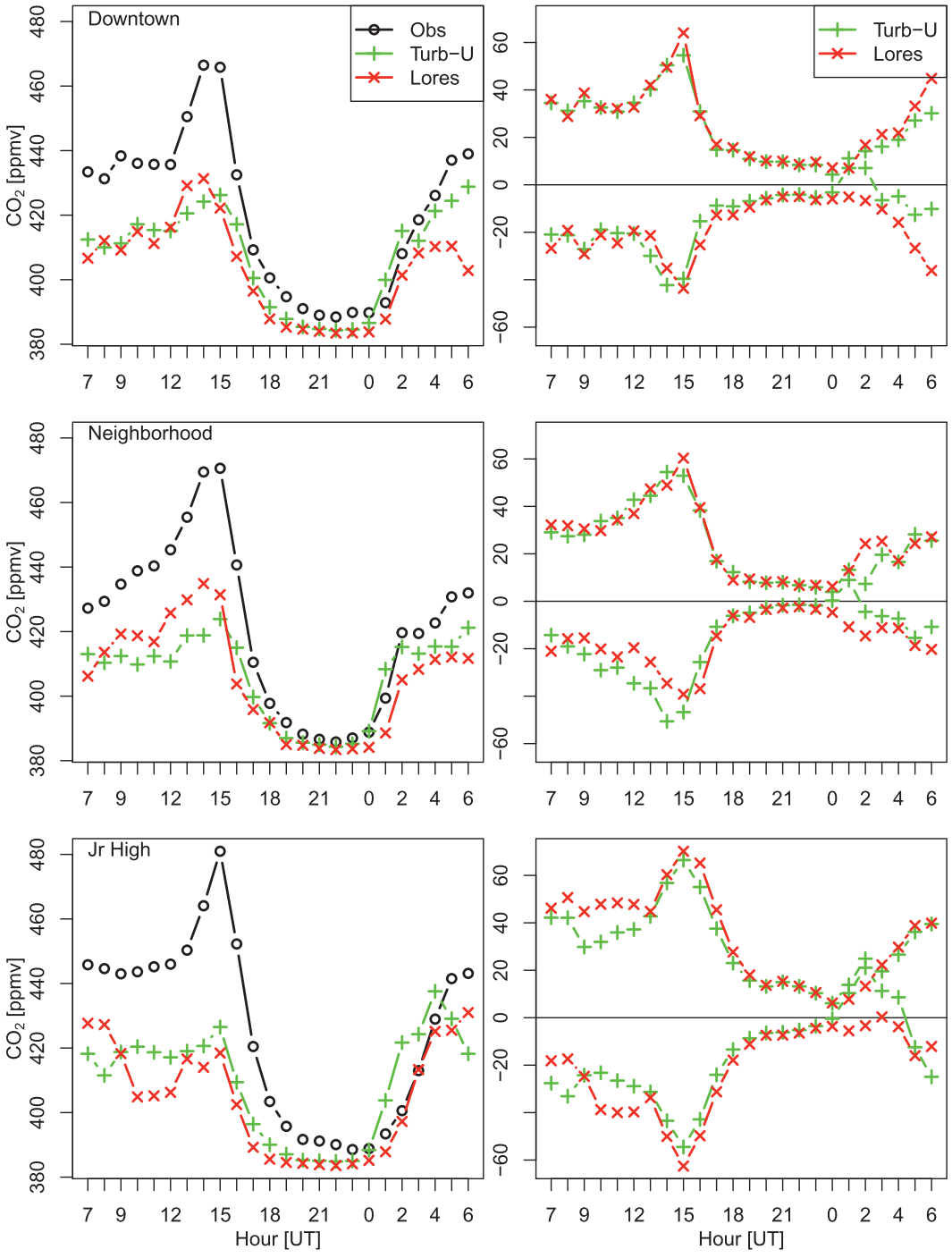

FIG. 15. Mean observed and modeled CO_2 concentrations for 2 weeks in October 2006, for three sites in SLC, as a function of time of day. Shown are (left) the values and (right) the corresponding bias and RMSE.

of simulations are systematically underpredicting CO_2 (caused by some combination of an overestimate of atmospheric mixing and an underestimate of anthropogenic sources). As is discussed in greater detail in McKain et al. (2012), the simulated concentrations can be corrected by using appropriate scaling factors, and changes in emissions between different time periods can be detected by a comparison of scaling factors. The analysis in McKain et al. (2012) demonstrated that using the higher-resolution (Turb-U) WRF fields resulted in more robust estimates of

scaling factors and, correspondingly, improved detection of emission changes.

4. Discussion and conclusions

WRF simulations were conducted in the SLC area for the purpose of modeling ground-based measurements of CO_2. Two intensive observing periods during VTMX 2000 were used to evaluate the performance of parameterizations of the planetary boundary layer and an urban canopy model. To accommodate the UCM, new land-use definitions were used for urban areas (three vs one urban category) that define the density of buildings in a variety of urban and suburban areas more precisely. The results reported here show that for urban locations in the Salt Lake valley, there was a clear benefit from parameterizing the urban canopy for simulation of the PBL and near-surface conditions, particularly for temperature evolution at night. When the UCM is used, the boundary layer collapses more quickly just after sundown, closer to the observed timing, than it does without an urban parameterization. Near-surface nighttime temperatures are also cooler when using the UCM, by as much as 5°C, and are also in better agreement with observations. These improvements are most notable during quiet synoptic conditions (IOP 7) when flow was driven by local circulations. In contrast, the UCM created little to no improvement during the more active periods with synoptically driven flow.

Differences between runs using different PBL schemes were more significant outside of urban areas, but neither the eddy diffusivity scheme (YSU) nor the turbulent kinetic energy scheme of vertical mixing (MYJ) produced consistently better results. Differences in the wind fields, whether attributable to different parameterizations of the boundary layer or different parameterizations of the urban environments, were mostly transient features that moved and evolved with the flow. Comparison of WRF forecasts with upper-air wind profiles from the VTMX field campaign showed virtually identical errors for all runs. Our results, particularly the comparison of WRF vertical wind profiles with VTMX wind profiles, confirm the findings of Zhong and Fast (2003) that high-resolution mesoscale models are capable of reproducing the local and mesoscale circulations that characterize the Salt Lake City environment.

The results from the VTMX WRF runs suggest that high-resolution meteorological models with a parameterization of the urban environment should be used for modeling the transport and dispersion of CO_2 in urban environments. This was confirmed by simulations for a 2-week period in October of 2006 for which runs were conducted using both a low-resolution (4-km resolution) and a high-resolution (1.33 km, with a UCM) model configuration. Results show clearly improved simulations of near-surface temperature but near-neutral impacts for simulated wind speed and near-surface moisture. The improved simulation of the diurnal cycle of near-surface temperature was also reflected in improved simulations of the observed CO_2 concentration by the WRF-STILT modeling system. These improvements were most evident in the modeling of the early evening rise in observed CO_2 concentration linked to the collapse of the daytime PBL. Statistical analysis of simulated concentrations (see McKain et al. 2012) also indicated that the high-resolution results provided more robust estimates that are suitable for detecting changes in emissions.

Acknowledgments. We thank two anonymous reviewers for helpful comments that improved the paper. We are grateful to Jerome Fast (Pacific Northwest National Laboratory) for providing us with VTMX2000 data and to John Horel (University of Utah) for providing us with surface-station data. Shawn Milrad (University of Kansas) performed an initial analysis of the data. The CO_2 data were obtained online (http://co2.utah.edu). Gridded analysis fields were obtained from the NARR Internet site. We gratefully acknowledge help provided by John Halley Gotway of the WRF-MET team at NCAR in setting up and adapting WRF-MET. This study was supported by Grants NNX11AG47G from the National Aeronautics and Space Administration (NASA) and ATM-0830916 from the National Science Foundation (NSF) to Harvard University and by Grant ATM-0836153 from the National Science Foundation to Atmospheric and Environmental Research, Inc., as well as by the U.S. intelligence community. Any opinions, findings, conclusions, or recommendations expressed in this material are those of the authors and do not necessarily reflect the views of the intelligence community, NSF, or NASA.

REFERENCES

Bougeault, P., and P. Lacarrere, 1989: Parameterization of orography-induced turbulence in a mesobeta–scale model. *Mon. Wea. Rev.,* **117,** 1872–1890.

Bowman, C., 2009: Moving from MM5 to WRF: What does it mean? *2009 Regional Smoke Management Meeting,* Spokane, WA, EPA. [Available online at http://yosemite.epa.gov/R10/airpage.nsf/smoke/09+meeting.]

Chen, F., and J. Dudhia, 2001: Coupling an advanced land-surface–hydrology model with the Penn State–NCAR MM5 modeling system. Part I: Model implementation and sensitivity. *Mon. Wea. Rev.,* **129,** 569–586.

——, and Coauthors, 2011: The integrated WRF/urban modeling system: Development, evaluation, and applications to urban environmental problems. *Int. J. Climatol.,* **31,** 273–288.

Chen, S.-H., and W.-Y. Sun, 2002: A one-dimensional time dependent cloud model. *J. Meteor. Soc. Japan,* **80,** 99–118.

Chin, H.-N. S., M. J. Leach, G. A. Sugiyama, J. M. Leone Jr., H. Walker, J. S. Nasstrom, and M. Brown, 2005: Evaluation of an urban canopy parameterization in a mesoscale model using VTMX and URBAN 2000 data. *Mon. Wea. Rev.,* **133,** 2043–2068.

Doran, J. C., J. D. Fast, and J. Horel, 2002: The VTMX 2000 campaign. *Bull. Amer. Meteor. Soc.,* **83,** 537–551.

Grell, G. A., and D. Dévényi, 2002: A generalized approach to parameterizing convection combining ensemble and data assimilation techniques. *Geophys. Res. Lett.,* **29,** 1693, doi:10.1029/2002GL015311.

Gurney, K. R., D. L. Mendoza, Y. Zhou, M. L. Fischer, C. C. Miller, S. Geethakumar, and S. de la Rue du Can, 2009: High resolution fossil fuel combustion CO_2 emission fluxes for the United States. *Environ. Sci. Technol.,* **43,** 5535–5541.

Holt, T., and J. Pullen, 2007: Urban canopy modeling of the New York City metropolitan area: A comparison and validation of single- and multilayer parameterizations. *Mon. Wea. Rev.,* **135,** 1906–1930.

Homer, C., C. Huang, L. Yang, B. Wylie, and M. Coan, 2004: Development of a 2001 national land cover database for the United States. *Photogramm. Eng. Remote Sens.,* **70,** 829–840.

Hong, S.-Y., Y. Noh, and J. Dudhia, 2006: A new vertical diffusion package with an explicit treatment of entrainment processes. *Mon. Wea. Rev.,* **134,** 2318–2341.

Hu, X.-M., J. W. Nielsen-Gammon, and F. Zhang, 2010: Evaluation of three planetary boundary layer schemes in the WRF model. *J. Appl. Meteor.,* **49,** 1831–1844.

Iacono, M. J., J. S. Delamere, E. J. Mlawer, M. W. Shephard, S. A. Clough, and W. D. Collins, 2008: Radiative forcing by long-lived greenhouse gases: Calculations with the AER radiative transfer models. *J. Geophys. Res.,* **113,** D13103, doi:10.1029/2008JD009944.

Janjić, Z. I., 2002: Nonsingular implementation of the Mellor–Yamada level 2.5 scheme in the NCEP Meso model. NCEP Office Note 437, 61 pp.

Jiménez, P. A., and J. Dudhia, 2012: Improving the representation of resolved and unresolved topographic effects on surface wind in the WRF model. *J. Appl. Meteor. Climatol.,* **51,** 300–316.

Lin, J. C., C. Gerbig, S. C. Wofsy, A. E. Andrews, B. C. Daube, K. J. Davis, and A. Grainger, 2003: A near-field tool for simulating the upstream influence of atmospheric observations: The Stochastic Time-inverted Lagrangian Transport (STILT) model. *J. Geophys. Res.,* **108,** 4493, doi:10.1029/2002JD003161.

Loridan, T., and C. Grimmond, 2012: Multi-site evaluation of an urban land-surface model: Intra-urban heterogeneity, seasonality and parameter complexity requirements. *Quart. J. Roy. Meteor. Soc.,* **138,** 1094–1113.

——, and Coauthors, 2010: Trade-offs and responsiveness of the single-layer urban canopy parametrization in WRF: An offline evaluation using the MOSCEM optimization algorithm and field observations. *Quart. J. Roy. Meteor. Soc.,* **136,** 997–1019.

McKain, K., S. C. Wofsy, T. Nehrkorn, J. Eluszkiewicz, J. R. Ehleringer, and B. B. Stephens, 2012: Assessment of ground-based atmospheric observations for verification of greenhouse gas emissions from an urban region. *Proc. Natl. Acad. Sci. USA,* **109,** 8423–8428.

Mellor, G. L., and T. Yamada, 1982: Development of a turbulence closure model for geophysical fluid problems. *Rev. Geophys. Space Phys.,* **20,** 851–875.

Nehrkorn, T., J. Eluszkiewicz, S. C. Wofsy, J. C. Lin, C. Gerbig, M. Longo, and S. Freitas, 2010: Coupled Weather Research and Forecasting–Stochastic Time-Inverted Lagrangian Transport (WRF-STILT) model. *Meteor. Atmos. Phys.,* **107,** 51–64.

National Research Council, 2010: *Verifying Greenhouse Gas Emissions: Methods to Support International Climate Agreements.* The National Academies Press, 124 pp. [Available online at http://www.nap.edu/openbook.php?record_id=12883.]

Otkin, J. A., and T. J. Greenwald, 2008: Comparison of WRF model-simulated and MODIS-derived cloud data. *Mon. Wea. Rev.,* **136,** 1957–1970.

Salamanca, F., A. Martilli, M. Tewari, and F. Chen, 2011: A study of the urban boundary layer using different urban parameterizations and high-resolution urban canopy parameters with WRF. *J. Appl. Meteor. Climatol.,* **50,** 1107–1128.

Skamarock, W. C., and J. B. Klemp, 2008: A time-split nonhydrostatic atmospheric model for Weather Research and Forecasting applications. *J. Comput. Phys.,* **227,** 3465–3485.

Yang, L., C. Huang, C. G. Homer, B. K. Wylie, and M. J. Coan, 2003: An approach for mapping large-area impervious surfaces: Synergistic use of *Landsat-7* ETM+ and high spatial resolution imagery. *Can. J. Remote Sens.,* **29,** 230–240, doi:10.5589/m02-098.

Zhong, S., and J. Fast, 2003: An evaluation of the MM5, RAMS, and Meso-Eta models at subkilometer resolution using VTMX field campaign data in the Salt Lake Valley. *Mon. Wea. Rev.,* **131,** 1301–1322.